An Inverse Spectral Method to Localize Discordant Alternans Regions on the Heart from Body Surface Measurements

Jaume Coll-Font[1], Burak Erem[1], Alain Karma[2], and Dana H. Brooks[1]

[1] B-Spiral Group, Dept. of ECE, Northeastern University, Boston, MA, USA
[2] Physics Dept., Northeastern University, Boston, MA, USA

Abstract. Spatially discordant T-wave alternans (TWA) has been shown to be linked to the genesis of ventricular fibrillation. Identification of discordant TWA through spatial characterization of TWA patterns in the heart has the potential to improve sudden cardiac death risk stratification. In this paper we present a method to solve a new variant of the inverse problem in electrocardiography that is tailored to estimate the TWA regions on the heart from non-invasive measurements on the body surface. We evaluate our method using both body surface potentials synthesized from heart surface potentials generated with ECGSIM and from potentials measured on a canine heart, and we show that this method detects the main regions in the heart undergoing TWA.

1 Introduction

Sudden cardiac death (SCD) is one of the leading causes of death in western countries. T-wave alternans (TWA), which is defined as beat-to-beat alternation in T-wave amplitude, has been linked to ventricular fibrillation (VF), one of the known causes of SCD [1, 2]. Thus noninvasive TWA detection is of considerable interest as a predictor of SCD risk, which currently have high sensitivity, but their specificity is only approximately 50% [3]. An additional limitation of current detectors is that they only report the presence or absence of TWA; they are unable to identify whether the detected TWA is due to a spatially heterogeneous (discordant) or homogeneous (concordant) distribution of alternations in the heart [4]. Discordant alternans is thought to excite reentrant spiral circuits that cause VF, which has been observed in computer simulations as well as in animal experiments [5–7]. Most of the previous work in the detection of discordant TWA has been focused on directly estimating TWA in heart potentials recorded from animal experiments or on the detection of patterns on the body surface that are characteristic of spatially discordant or concordant alternans [7–9]. In an approach relating the body surface measurements to the heterogeneities on the heart, Sassi *et al.* used a first order Taylor approximation of the T-wave to extract an index of the action potential duration (APD) variability on the heart [10,11]. Janusek *et al.* also published a study where they used the ECGSIM model (www.ecgsim.org) to simulate APD alternation distributions that matched their observations on the body [12, 13].

S. Ourselin, D. Rueckert, and N. Smith (Eds.): FIMH 2013, LNCS 7945, pp. 241–248, 2013.

In this paper, we propose a method of characterizing the spatial distribution of TWA on the heart from body surface measurements and a model of the heart-torso geometry by posing an inverse problem. We explicitly employ the temporal characteristics of TWA as a regularization method. In particular, our method differs from these previous approaches in that we estimate the spatial distribution of the alternations on the heart without assuming any model for the cellular basis of the TWA generation (*e.g.* APD alternation).

This paper first introduces some background theory in Sec. 2 on the standard Spectral Method and forward and inverse methods. Using these as a base, we explain our inverse spectral method for TWA detection in Sec. 3. Sec. 4 presents experimental results, and a discussion on the algorithm and results is presented in Sec. 5.

2 Background

In this section we will describe the standard spectral method to detect T-wave alternans from body surface potential measurements, and in brief, the forward and inverse problems of electrocardiography.

2.1 Spectral Method

The Spectral Method (SM) is the most widely used TWA detection method [14, 15]. It assumes that time-aligned T-waves from a sequence of beats will exhibit beat-to-beat alternations in potential amplitude at equivalent sample times. Therefore the method computes a beat-to-beat Fourier transform at each time sample during the T-wave and analyzes the beat-frequency spectrum at each sample time for high amplitude oscillations with a period of 2 beats [16]. Mathematically, we can describe this method by first creating an order 3 tensor $\mathcal{T}_{l,t,b}$ with the segmented T-waves such that each entry corresponds to the potential at electrode l, sample time t and beat index b. On this structure, the SM performs a Fourier transform in the beat index:

$$\mathcal{F}_{l,t,f} = \sum_{b=0}^{B-1} \mathcal{T}_{l,t,b} e^{j2\pi fb/B}. \tag{1}$$

Since the method searches for period 2 oscillations, the Spectral Method constrains the previous transform to frequency $f = \frac{1}{2}$ resulting in a matrix with elements: $\mathcal{B}_{l,t} = \mathcal{F}_{l,t,\frac{1}{2}}$. A typical TWA detector computes a single score from the matrix of Fourier transform coefficients and compares its value to a predetermined threshold [1, 17].

2.2 Forward and Inverse Problems

The relationship between potentials on the heart and the corresponding body surface potentials can be calculated from geometrical and tissue conductivity

modeling. Extracting this relationship solves the "forward problem" [18]. From electromagnetic theory it can be shown that this relation between heart potentials x_t and body surface potentials y_t is linear and static in time; thus the forward solution determines the matrix A that defines the linear operator.

$$y_t = Ax_t \tag{2}$$

The problem of estimating the heart potentials from the body surface potentials is called the inverse problem [19]. Because of the characteristics of the forward propagation of potentials from heart to torso surface, the matrix A in (2) is ill-conditioned, and thus the solutions to the inverse problem need regularization. A classical method of regularizing this problem is Tikhonov regularization, which consists of solving:

$$min_{x_t}\|y_t - Ax_t\|_2^2 + \lambda_t\|Rx_t\|_2^2 \tag{3}$$

In Tikhonov regularization, the parameter $\lambda_t > 0$ determines the amount of regularization imposed and the regularization matrix R determines the type of regularization. Typical choices of R are the identity matrix, which tends to make solutions small, and approximations to the Laplacian operator on the heart, which tend to make solutions smooth [20].

3 Methods

This section explains our proposed method to estimate TWA epicardial distributions. It is composed of two main blocks, the temporal regularization and the inverse solution method. The temporal regularization is itself composed of two parts, a spectral method calculation on the body surface data and a projection to a low frequency Fourier basis. The input to the algorithm is a sequence of B T-waves of length T sorted in a matrix Y, whose rows represent the electrode index l and columns represent the sample time t. Then we can build a sparse matrix $\mathcal{S}_{SM,f}$ such that the multiplication $\mathcal{B} = Y\mathcal{S}_{SM,f}$ is equivalent to applying the SM to the data, as in (1). The structure of this matrix is given by $\mathcal{S}_{SM,f} = I \otimes \mathcal{S}_{f,B}$ where I is the identity matrix of size T and $\mathcal{S}_{f,B}$ is:

$$\mathcal{S}_{f,B} = [1, e^{j2\pi f\frac{1}{B}}, \cdots, e^{j2\pi f\frac{B-1}{B}}]^T \in \mathbb{C}^B. \tag{4}$$

Then, the resulting matrix $\mathcal{B}$ are the same time varying Fourier coefficients as in Sec. 2.1. To further regularize the problem, $\mathcal{B}$ is Fourier transformed over time as well, and truncated to low frequencies in order to take advantage of the low frequency nature of the T-wave signal. As in the previous step, this computation can be done with a right matrix multiplication, $\tilde{Y} = \mathcal{B}\mathcal{S}_{f,T}$, with $\mathcal{S}_{f,T}$ as defined in (4). Thus, by the associative property, we can state the relationship between the low-frequency Fourier coefficients of the SM applied to body surface potentials, $\tilde{Y}$, and heart surface potentials, $\tilde{X}$, as:

$$\begin{aligned}(Y\mathcal{S}_{SM,\frac{1}{2}}\mathcal{S}_{f,T}) =& A(X\mathcal{S}_{SM,\frac{1}{2}}\mathcal{S}_{f,T})\\ \tilde{Y} =& A\tilde{X}.\end{aligned} \tag{5}$$

To solve for the low-frequency Fourier coefficients of the SM on the heart surface potentials, we solve the inverse problem using Tikhonov regularization as explained in Sec. 2.2, where the λ parameter is computed by choosing the value at the corner of an L-curve [21] and the regularization matrix is chosen as either the identity matrix or a 3D Laplacian operator on a combined epicardial/endocardial heart surface [20]. Finally, we reconstruct the SM waveform on the heart surface from its low-frequency Fourier coefficients, which can be compared to the results of the SM directly applied to the heart surface signals, when such data are available.

4 Experiments

In order to evaluate the capacity of our algorithm to characterize the spatial distribution of TWA we have tested it on two different types of datasets. The first type was composed of series of 128 heartbeats created with synthetic heart potentials derived from the mathematical model in ECGSIM [12]. The examples were interactively generated in the simulation package SCIRUN [22, 23] by generating APD alternation ($\pm$20 ms) in chosen regions of the heart in both endocardium and epicardium. This model allowed us to have complete control over the amplitude and spatial distribution of the TWA, giving us a broad set of cases to test and a well defined ground truth to compare to.

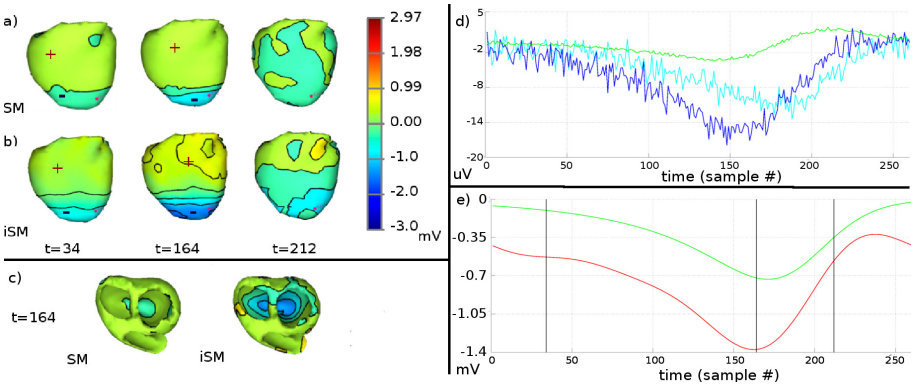

Fig. 1. Example of results for an ECGSIM case with TWA in the apex. a) and b) show the anterior side of the heart three consecutive time instances for the SM reference and the inverse solution respectively. The corresponding time instances are marked with vertical lines in e) with the time waveforms of SM reference (green) and inverse solution (red) corresponding to the node marked in pink on the heart images. Image c) shows the solutions of the endocardium for a single time instance, here left is SM and right is inverse SM. Finally, d) shows an example of two consecutive beats (blue and cyan) and the iSM estimated TWA (green) on lead V2.

The second dataset consisted of a single case of 84 heartbeats of measured canine epicardial potentials recorded during an open chest experiment where ischemia was induced by occluding the LAD artery. TWA was observed in this dataset but we do not have a well defined ground truth region because our assessment depends on the application of the SM to noisy measurements.

For all cases the procedure was the following: First we forward propagated the heart potentials to the body surface using forward matrices obtained from human torso and heart geometries. Then we added white Gaussian noise with a power 15 dB below the rms of the simulated body surface signals during QRST interval and we applied our method. A major difference between the ECGSIM and the canine heart cases is that for the first we had endocardial surface data, but not for the second. As a result, for the ECGSIM cases, we regularized with a 3D Laplacian matrix in order to detect epicardial and endocardial alternations, for the canine case, we used an identity regularizer to detect epicardial TWA. For comparisons, we also computed the Spectral Method on the heart potentials as described in Sec. 2.1.

Figure 1 shows an example of results in an ECGSIM case with discordant alternans regions on the epicardial and endocardial surfaces of the apex. Row a) shows the isopotential maps from the SM applied directly to the heart data for 3 sample times during the T-wave. Row b) shows the corresponding results of our method (iSM). For this same experiment, the endocardial results are shown in (c) and the waveforms corresponding to a node on the epicardial surface of the apex, marked with a pink dot, are in (e). In (d), we show an example of two consecutive noisy T-waves in body surface lead V2, after time alignment, with the corresponding TWA magnitude in green.

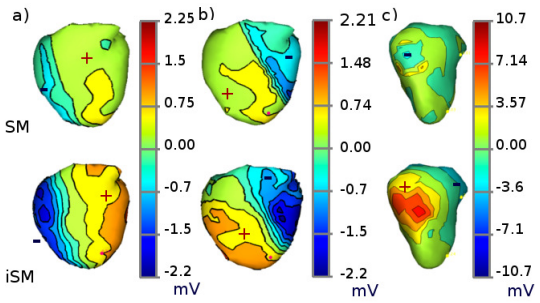

Fig. 2. Example of the anterior view of the spatial distributions of TWA for three different cases (a,b,c) generated with ECGSIM model. Top row shows SM reference (SM) and bottom row the inverse solution (iSM).

Three more examples of different spatial distributions of TWA are shown in Fig. 2, all taken at sample times at the peak of their respective TWA amplitudes. The top row is the SM reference and the bottom row is the inverse estimate.

The results on the canine data are shown in Fig. 3. We show the spatial distribution of TWA for a single time instance from both front and back views, as well as the temporal waveforms for the nodes marked in pink, as before. The rows are organized as in the previous figure.

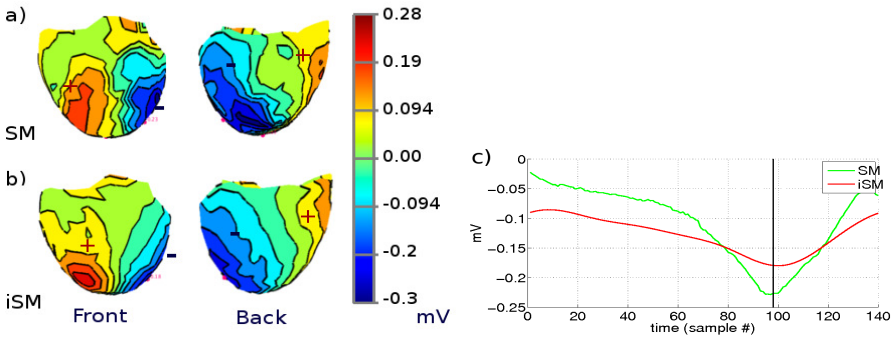

Fig. 3. Example of the spatial distributions of TWA for a single time instance in the canine experiment. (a) shows SM reference (SM) and (b) the inverse solution (iSM). In (c) are shown the amplitude of the TWA over time for the node marked in pink on the heart. The green line is SM reference, the blue line is the inverse solution and the black line indicates the sampling time of the images in (a) and (b).

5 Discussion

The results shown in Fig. 1 are representative of typical results obtained in our experiments with ECGSIM cases. In this figure, we observe two well defined discordant regions with both our method and the SM applied to heart data, and the regions identified by both methods are largely congruent. The boundaries of the regions are generally constant across time, although the edges of the regions recovered by iSM are a blurred version of the results obtained by applying the SM to heart potentials directly. The algorithm also detects the presence of TWA in the endocardium, although with some loss of spatial accuracy compared to the epicardium. An example waveform is shown in Fig. 1 c) and is similar to the waveforms obtained for other nodes, with variations in amplitude, phase and sign. Even though the low-frequency approximation captures the behavior of the waveforms, the amplitudes at each time and location do not exactly match and may need additional refinement.

For most cases, as shown in the examples in Fig. 2 a) and b), the detected alternating regions generally matched those of the SM. However, the algorithm has some limitations when trying to detect small discordant regions. An example of this can be seen in Fig. 2 c), where the algorithm has failed to detect the alternating region and instead finds TWA of opposite phase in a broader area surrounding the affected region. We believe these errors have two main sources: the first is the inverse method, which fails to detect small regions whose effect on the body surface has small amplitudes and is thus concealed by noise. The second is the spectral method itself, which also has troubles detecting this discordant region when applied directly to the heart potentials. The second part of this can be seen clearly in the top image in Fig. 2 c), where the true TWA region is in light blue (labeled with a "-" symbol), but the SM detects a higher amplitude alternations at the borders of the region than within it.

For the canine experiment shown in Fig. 3, the detected regions in both the inverse solution and the spectral method are broad and spatially smooth. As in the ECGSIM cases, both methods agree on the main alternating areas while there are differences on the exact region boundaries. The smoothness of the results in both cases highlights a temporal resolution problem in the SM that is inherited by the inverse SM. That is, to compute a reliable Fourier transform as part of both methods, one needs enough beats to average out noise effects. However, variations in the TWA distribution or timing during these beats may be causing spatial smoothing of the alternating regions. This variations of timing can be taken into account by instead averaging even and odd beats separately with the technique in [24] and then taking their difference as the TWA measure. In terms of temporal behavior, as shown in Fig. 3 c), the shapes of the waveforms are quite similar in both methods, but their amplitudes differ. The main differences between them occur at the peak of the waveform where our inverse solution, due to regularization towards lower frequencies, fails to match the sharper shape of the waveform obtained with the SM.

In conclusion, the inverse problem and solution method proposed here, including the two types of temporal regularization, may help to localize the major areas affected by TWA on the heart. In the future, we plan to further study this method and its potential utility as a predictor of VF.

Acknowledgments. This work has been funded in part by a tier 1 seed grant from the office of the Northeastern University Vice Provost for Research and by grant 8 P41 GM103545-14 from the National Institutes of Health. The authors would like to thank Kedar Aras, Brett Burton and Rob MacLeod from the center CVRTI for providing the data from the canine experiments.

References

1. Rosenbaum, D., Jackson, L., Smith, J., Garan, H., Ruskin, J., Cohen, R.: Electrical alternans and vulnerability to ventricular arrythmias. New. Engl. J. Med. 330(4), 235–241 (1994)
2. Romero, I., Grubb, N., Clegg, G., Robertson, C., Addison, P., Watson, J.: T-wave alternans found in preventricular tachyarrhythmias in CCU patients using a wavelet transform-based methodology. IEEE T. Bio-Med. Eng. 55, 2658–2665 (2008)
3. Hunt, A.: T Wave Alternans in high arrhythmic risk patients: analysis in time and frequency domains: a pilot study. BMC Cardiov. Dis. 2, 6 (2002)
4. Martínez, J., Olmos, S.: Methodological principles of T wave alternans analysis: a unified framework. IEEE T. Bio-Med. Eng. 52, 599–613 (2005)
5. Karma, A.: Electrical alternans and spiral wave breakup in cardiac tissue. Chaos 4(3), 461–472 (1996)
6. Weiss, J., Karma, A., Shiferaw, Y., Chen, P., Garfinkel, A., Qu, Z.: From pulsus to pulseless: the saga of cardiac alternans. Circ. Res. 98(10), 1244–1253 (2006)
7. Pastore, J.M., Girouard, S.D., Laurita, K.R., Akar, F.G., Rosenbaum, D.S.: Mechanism linking T-wave alternans to the genesis of cardiac fibrillation. Circ. 99, 1385–1394 (1999)

8. Martínez, J., Olmos, S., Wagner, G., Laguna, P.: Characterization of repolarization alternans during ischemia: time-course and spatial analysis. IEEE T. Bio-Med. Eng. 53, 701–711 (2006)
9. Janusek, D., Kania, M., Zaczek, R., Zavala-Fernandez, H., Zbieć, A., Opolski, G., Maniewski, R.: Application of Wavelet Based Denoising for T-Wave Alternans Analysis in High Resolution ECG Maps. Meas. Sci. Rev. 11, 181–184 (2011)
10. Sassi, R., Mainardi, L.: Refined Estimate of the Dominant T-Wave. Cinc. (5), 845–848 (2010)
11. Sassi, R., Mainardi, L., Cerutti, S.: Amplitude of Dominant T Wave Alternans assessment on ECGs obtained from a biophysical model. In: EMBS, vol. (8), pp. 5872–5875 (September 2011)
12. Oostendorp, T., van Oosterom, A.: Ecgsim: an interactive tool for the study of the relation between the electric activity of the heart and the qrst waveforms at the body surface. In: IEMBS, vol. 2, pp. 3559–3562 (September 2004)
13. Janusek, D., Kania, M., Kepski, R., Maniewski, R.: Simulation of T-Wave Alternans and its Relation to the Duration of Ventricular Action Potentials Disturbance. Therapy, 21–27 (2010)
14. Adachi, K., Ohnishi, Y., Shima, T., Yamashiro, K., Takei, A., Tamura, N., Yokoyama, M.: Determinant of microvolt-level t-wave alternans in patients with dilated cardiomyopathy. J. Am. Coll. Cardiol. 34(2), 374–380 (1999)
15. Gold, M., Bloomfield, D., Anderson, K., El-Sherif, N., Wilber, D., Groh, W., Estes, N.R., Kaufman, E., Greenberg, M., Rosenbaum, D.: A comparison of t-wave alternans, signal averaged electrocardiography and programmed ventricular stimulation for arrhythmia risk stratification. J. Am. Coll. Cardiol. 36(7), 2247–2253 (2000)
16. Smith, J., Clancy, E.A., Valeri, C., Ruskin, J., Cohen, R.: Electrical alternans and cardiac electrical instability. Circ. 77, 110–121 (1988)
17. Madias, J.: T-wave alternans and the confounding role of the T-wave amplitude. Journal of Electrocardiology 45, 294–295 (2012)
18. MacLeod, R., Buist, M.: The forward problem of electrocardiography. In: Comp. Elec. Springer (2010)
19. Pullan, A., Cheng, L., Nash, M., Ghodrati, A., MacLeod, R., Brooks, D.: The inverse problem of electrocardiography. In: Comp. Elec. Springer (2010)
20. Erem, B., Brooks, D.: Differential geometric approximation of the gradient and hessian on a triangulated manifold. In: ISBI (2011)
21. Hansen, C.: Regularization tools: A matlab package for analysis and solution of discrete ill-posed problems. Numerical Algorithms 6(1), 1–35 (1994)
22. SCI Institute, SCIRun: A Scientific Computing Problem Solving Environment, Scientific Computing and Imaging Institute (SCI) (2013), `http://www.scirun.org`
23. MacLeod, R., Stinstra, J., Lew, S., Whitaker, R., Swenson, D., Cole, M., Krueger, J., Brooks, D., Johnson, C.: Subject-specific, multiscale simulation of electrophysiology: a software pipeline for image-based models and application examples. Philos. T. R. Soc. A 367(1896), 2293–2310 (2009)
24. Martínez-Orellana, R., Erem, B., Brooks, D.H.: Time Invariant Multielectrode Averaging For Biomedical Signals. In: ICASSP (2013)